

ORIGINAL RESEARCH

Open Access



Exploring the impact of PEGylation on pharmacokinetics: a size-dependent effect of polyethylene glycol on prostate-specific membrane antigen inhibitors

Yang Liu^{1,2,3}, Li Xia^{1,2,4}, Haiyang Li^{1,2,4}, Ping Cai^{1,2,4}, Sufan Tang^{1,2,4}, Yue Feng^{1,2,3}, Guangfu Liu^{1,3}, Yue Chen^{1,2,3*}, Nan Liu^{5*}, Wei Zhang^{5*} and Zhijun Zhou^{1,2,3,4*}

Abstract

Background Prostate cancer is the second most frequent cancer and the fifth leading cause of cancer-related deaths in men. Prostate-specific membrane antigen (PSMA) as a target has gained increasing attention. This research aims to investigate and understand how altering size of PEG impacts the in vitro and in vivo behavior and performance of PSMA inhibitors, with a specific focus on their pharmacokinetic characteristics and targeting properties.

Results Two ⁶⁸Ga-labeled PSMA-targeted radiotracers were developed, namely [⁶⁸Ga]Ga-PP4-WD and [⁶⁸Ga]Ga-PP8-WD, with varying sizes of polyethylene glycol (PEG). [⁶⁸Ga]Ga-PP4-WD and [⁶⁸Ga]Ga-PP8-WD had excellent affinity for PSMA with IC₅₀ being 8.06 ± 0.91, 6.13 ± 0.79 nM, respectively. Both tracers enabled clear visualization of LNCaP tumors in PET images with excellent tumor-to-background contrast. They also revealed highly efficient uptake and internalization into LNCaP cells, increasing over time. The biodistribution studies demonstrated that both radioligands exhibited significant and specific uptake into LNCaP tumors. Furthermore, they were rapidly cleared through the renal pathway, as evidenced by [⁶⁸Ga]Ga-PP4-WD and [⁶⁸Ga]Ga-PP8-WD showing a tenfold and a fivefold less in renal uptake, respectively, compared to [⁶⁸Ga]Ga-Flu-1 in 30 min. Both in vitro and in vivo experiments demonstrated that PEG size significantly impacted tumor-targeting and pharmacokinetic properties.

Conclusions These radiotracers have demonstrated their effectiveness in significantly reducing kidney uptake while maintaining the absorbed dose in tumors. Both radiotracers exhibited strong binding and internalization characteristics in vitro, displayed high specificity and affinity for PSMA in vivo.

Keywords Prostate-specific membrane antigen (PSMA), Prostate cancer (PCa), Polyethylene glycol (PEG), LNCaP, Micro-PET/CT

*Correspondence:

Yue Chen
chenyue5523@126.com

Nan Liu
liunan_815@163.com

Wei Zhang
zhangwscd@uestc.edu.cn

Zhijun Zhou
zhouzjiang@gmail.com

Full list of author information is available at the end of the article



© The Author(s) 2024. **Open Access** This article is licensed under a Creative Commons Attribution 4.0 International License, which permits use, sharing, adaptation, distribution and reproduction in any medium or format, as long as you give appropriate credit to the original author(s) and the source, provide a link to the Creative Commons licence, and indicate if changes were made. The images or other third party material in this article are included in the article's Creative Commons licence, unless indicated otherwise in a credit line to the material. If material is not included in the article's Creative Commons licence and your intended use is not permitted by statutory regulation or exceeds the permitted use, you will need to obtain permission directly from the copyright holder. To view a copy of this licence, visit <http://creativecommons.org/licenses/by/4.0/>.

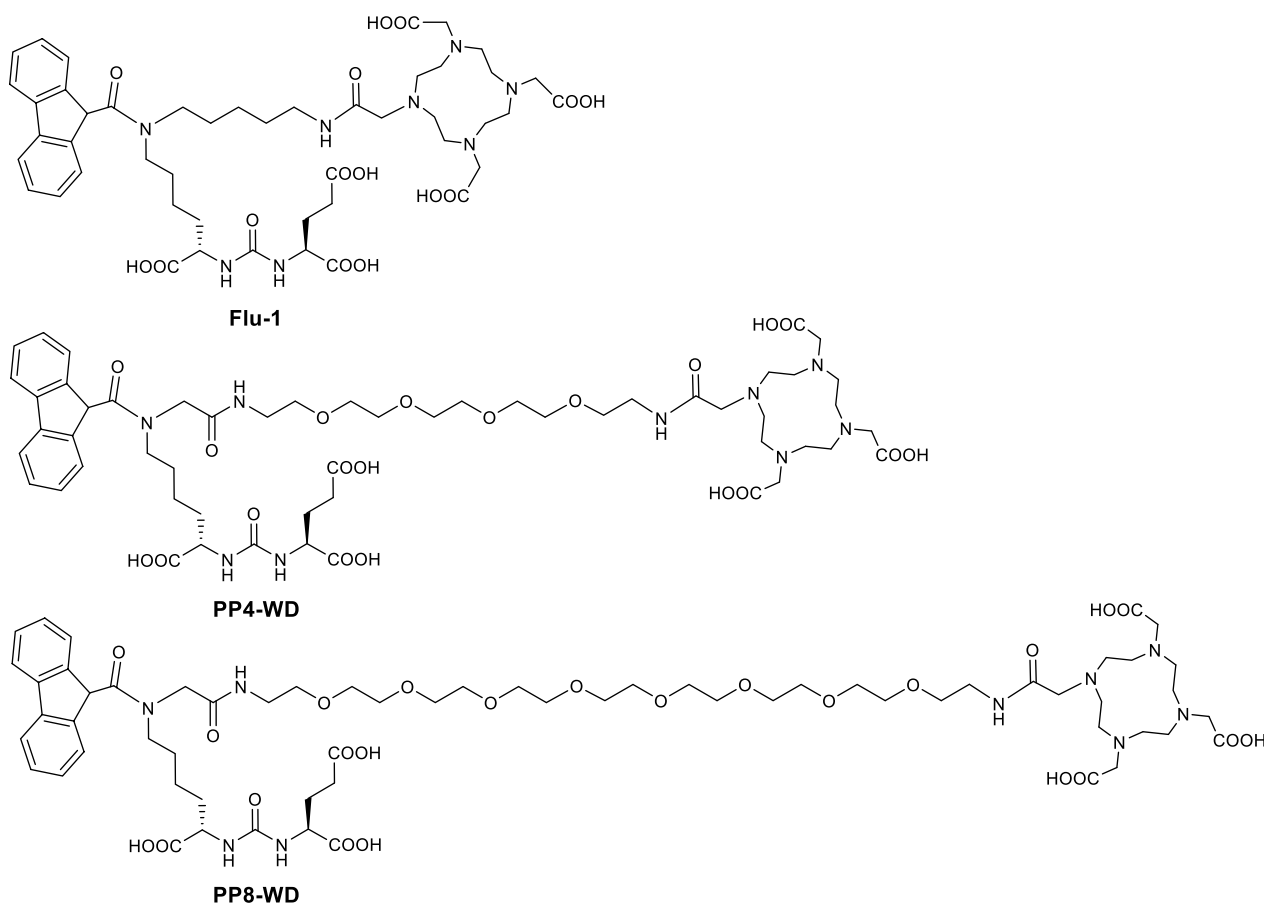


Fig. 2 The chemical structures of Flu-1, PP4-WD, and PP8-WD

amounts of $^{68}\text{GaCl}_3$ (18.5–40 MBq) in sodium acetate buffer (NaAc/HAc=0.5 M/0.5 M) and heating the solution at 95 °C for 15 min. The reaction mixture was then diluted with 4 mL of saline and purified through a pre-activated Oasis HLB column, followed by washing with 5 mL of saline. The final product was eluted with 100 μL of 50% ethanol and diluted with 400 μL of physiological saline. The radiochemical purity was determined by RP-HPLC.

^{177}Lu -radiolabeling

^{177}Lu was provided by the Institute of Nuclear Physics and Chemistry at the China Academy of Engineering Physics (Mianyang, China). A quantity of $^{177}\text{LuCl}_3$ (37–74 MBq) was transferred to a reaction vial containing 5–10 μg of the corresponding conjugate, along with 0.25 M sodium acetate buffer (NaAc/HAc=0.5 M/0.5 M). The mixture was subjected to heat via vibration in a metal thermostatic bath at 95 °C for 15 min. Following this, the cooled reaction solution underwent filtration with sterile water using a pretreated Oasis HLB column. Radioactive purity was determined through RP-HPLC with 50% ethanol as

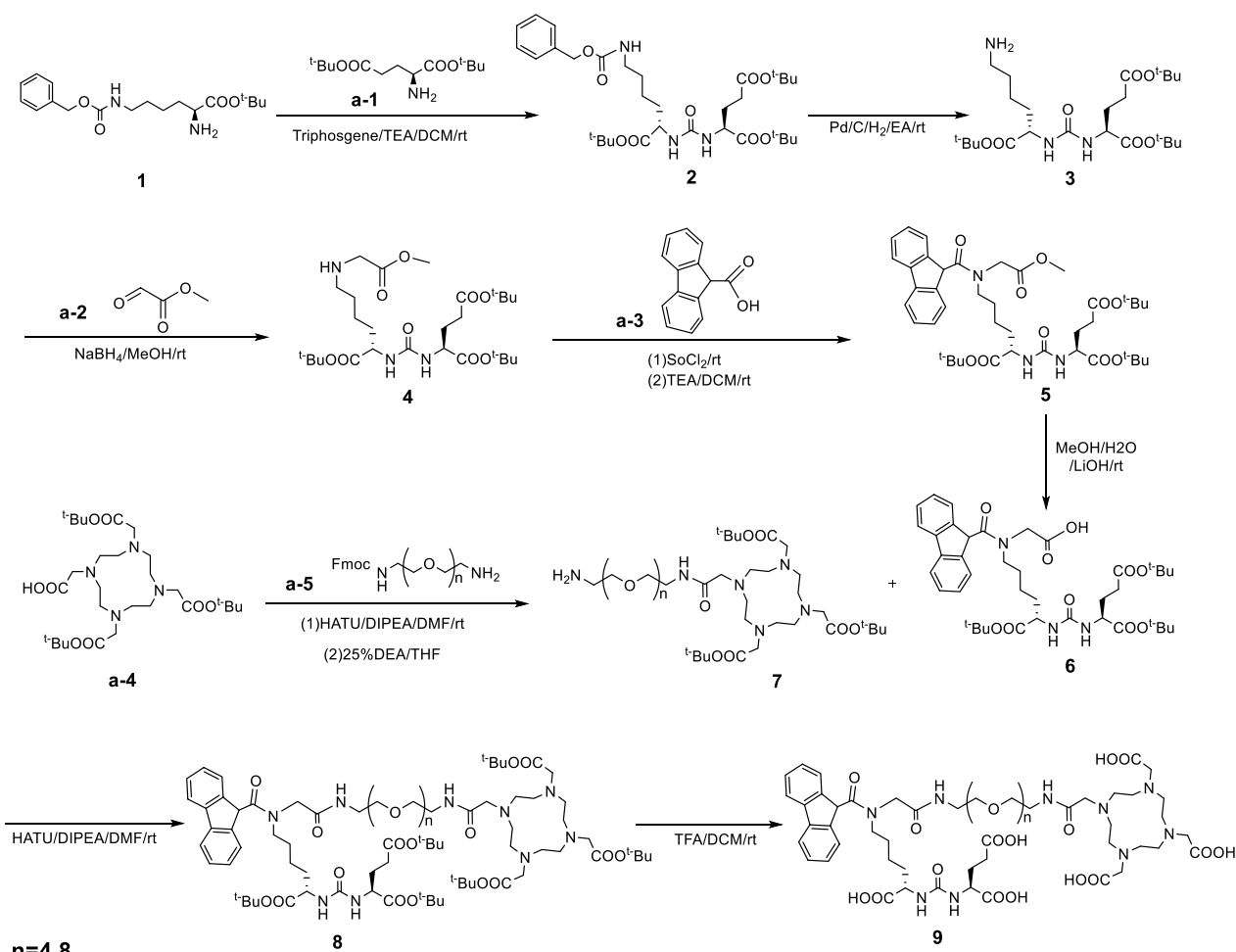
the elution solvent, and the resulting solution was subsequently diluted with physiological saline.

^{nat}Ga -labeled standards

To prepare ^{nat}Ga -labeled standards, a solution of PP4-WD (0.59 mg, 0.5 μmol) or PP8-WD (0.68 mg, 0.50 μmol), was incubated with ultrapure $^{nat}\text{Ga(III)}$ -chloride (Aladdin, China) (40 eq.) in 0.25 M sodium acetate buffer (NaAc/HAc=0.5 M/0.5 M) (200 μL) and 0.05 M HCl (800 μL) at 95 °C for 15 min. The reaction mixture was then purified by RP-HPLC, and the RP-HPLC eluates containing the desired compound were collected, pooled, and lyophilized.

Radiochemical stability

To investigate the stability of the ^{68}Ga -labeled compounds, [^{68}Ga]Ga-PP4-WD and [^{68}Ga]Ga-PP8-WD were incubated in either phosphate-buffered saline (PBS) or human serum at 37 °C for 30, 60, and 120 min in a shaking incubator. The radiochemical purity of samples incubated in PBS at each time point was determined using RP-HPLC. For the samples in human serum, a



Scheme 1 Synthesis of PP4-WD, PP8-WD. (PP4-WD: where n=4, PP8-WD: where n=8)

pretreatment step was applied. Briefly, the human serum samples underwent precipitation with acetonitrile, and the radiochemical purity of each supernatant aliquot was determined using RP-HPLC after centrifugation for 5 min at 10,000 rpm. The experiments were performed in triplicate.

Competitive cell binding assay

LNCaP prostate cancer cell line obtained from the American Type Culture Collection (ATCC, Manassas, VA) was used for cell affinity studies. The cells were grown in a meilunbio RPMI 1640 medium (ATCC modified) supplemented with 10% fetal bovine serum and 1% streptomycin/penicillin (Thermo Fisher Scientific, USA) at 37 °C in a humidified 5% CO₂ atmosphere. Two days (48 ± 2 h) prior to in vitro experiments, the cells were harvested using trypsin-ethylenediaminetetraacetic acid (EDTA; 0.25% trypsin, 0.02% EDTA) in PBS and centrifuged. The supernatant was disposed, and the cell pellet was resuspended in a culture medium, and LNCaP cells

(150,000 cells/well) were counted with a hemocytometer and seeded in poly-L-lysine-coated 24-well plates used in cell binding studies. The cells were then allowed to grow at 37 °C for 48 h. PC3-PIP cells provided by Professor Xiaoyuan Chen (Singapore) require additional Puromycin (2 µg/ml) in addition to the appealed culture conditions. Detailed information regarding uptake and internalization experiments can be found in the previous report [26].

In order to determine the binding affinity, a competitive cell binding assay was performed. LNCaP cells (100,000 cells/well) seeded in 96-well plates were incubated with a 0.185 MBq/50 µL solution of [⁶⁸Ga]Ga-PSMA-11 in the presence of eight different concentrations of ^{nat}Ga-PP4-WD or ^{nat}Ga-PP8-WD (0–10,000 nM, 50 µL/well). After incubation for 1 h at 37 °C, the cells were washed with ice-cold PBS three times and lysed with 1 M NaOH. The total radioactivity in each well was measured with a gamma counter. The 50% inhibitory concentration (IC₅₀) values were calculated by fitting the data using a

nonlinear regression algorithm (GraphPad Prism Software). Experiments were performed at least three times including quadruplicate sample measurements.

Log $D_{7.4}$

10 μL of each ^{68}Ga -radiolabeled compound (~ 0.037 MBq) were added to a vial containing 500 μL of octanol and 490 μL of 0.01 M PBS (pH=7.4). After vortexed for 5 min and centrifuging for 10 min (5000 rpm), the radioactive count of the octanol and PBS phases were determined with a γ -counter (CAPRAC-t, Edmonton, Canada). Log $D_{7.4}$ was then determined using the following equation: $\text{Log } D_{7.4} = \text{Log} [(\gamma \text{ counts in the octanol phase} - \gamma \text{ counts in background}) / (\gamma \text{ counts in PBS} - \gamma \text{ counts in background})]$. Each group was repeated 3 times, and the average value was expressed as $\log D_{7.4} \pm$ standard deviation (SD).

Biodistribution and imaging studies

All animal experiments were performed with the approval of the institutional animal ethics committee. Male NOD/SCID mice (5–6 weeks old) implanted with LNCaP cells were used for imaging and biodistribution experiments as previously described [27]. The mice were imaged or used in biodistribution studies once the tumor grew to 8–10 mm in diameter over a period of 4–5 weeks. At the same time, male balb/c-nu mice (5–6 weeks old) implanted with PC3-PIP cells were used as an alternative tumor model for imaging and biodistribution experiments.

To perform imaging studies, the male mice bearing LNCaP tumors were injected with the corresponding radioligand (~ 2.5 MBq; 100 μL) via their tail veins. The micro-PET/CT scans (Inveon PET, Siemens) were conducted at 10, 30, 60, and 120 min after injection. The mice were anesthetized and maintained under 2% isoflurane in oxygen at a flow rate of 2 L/min during the 2-h imaging study. First, a 10 min static PET imaging acquisition was carried out, followed by a 10 min CT scan for localization and attenuation correction. Data analysis was performed using Inveon Research Workplace software. For PC3-PIP tumor model, the imaging studies were performed with micro-PET/SPECT/CT (Inliview-3000B, Novel Medical). Data analysis was performed using Nmsoft-AI ws v1.7–1 software.

To conduct biodistribution studies, male mice bearing LNCaP or PC3-PIP tumors with an average body weight of approximately 20 ± 5 g and a tumor diameter of 8–10 mm were administered a bolus injection of 2.5 MBq of the corresponding radioligand via the tail vein. After 30, 60, and 120 min, the mice were anesthetized with isoflurane and subsequently euthanized by CO_2 asphyxiation. Blood was drawn, and the organs

of interest were promptly harvested, blotted dry, and weighed. The radioactivity of the collected mouse organs was measured and expressed as the percentage of the injected dose per gram of tissue (%ID/g). Each group consisted of at least five mice.

Results

Chemical and radiochemical synthesis and characterization

As shown in Scheme 1, the synthesis of these precursors through multiple step reactions is quite straightforward. We first constructed urea-based compound **2** bearing protected glutamate and lysine residues, followed by hydrogenation of compound **2** to yield compound **3**. Next, compound **3** underwent nucleophilic addition reaction with methyl glyoxylate, forming an imine, which was then reduced by NaBH_4 to provide compound **4**. Compound **5** was obtained by reacting **4** with 9-carboxyfluorene, then the methyl group was removed to yield compound **6**. The conjugation of compound **6** with the DOTA chelator was achieved through an amidation reaction, followed by the removal of the Fmoc-protective group under alkaline conditions to obtain compound **7**. Subsequently, compounds **6** and **7** were subjected to an amidation reaction followed by deprotection in trifluoroacetic acid. Finally, the target molecule was purified using RP-HPLC, resulting in a purity of over 95% for both precursors. PP4-WD and PP8-WD were characterized by ESI+Mass and had retention times at 8.0 min and 8.3 min on RP-HPLC, respectively (Additional file 1: Fig. S1–S2, Fig. 3A).

^{68}Ga labeling

The synthesis of ^{68}Ga -labeled PSMA inhibitors was achieved by reacting PP4-WD or PP8-WD with $^{68}\text{GaCl}_3$ in NaAc/HAc (v/v=1/1 with pH=4.3) buffer solution within 15 min at 95 $^\circ\text{C}$. ^{68}Ga labeling efficiency of both precursors analyzed with RP-HPLC for both ^{68}Ga -labeled PSMA inhibitors are >95%. After purification with Oasis HLB 1 cc (10 mg) extraction cartridges (Waters, USA), the radiochemical purity (RCP) for both radioligands then exceeded 98%. The retention times for [^{68}Ga]Ga-PP4-WD and [^{68}Ga]Ga-PP8-WD were 8.0 min and 8.1 min, respectively (Fig. 3B).

Lipophilicity

Hydrophilicity of these radioligands were investigated by measuring the partition coefficient ($\text{Log } D_{7.4}$) between octane and PBS. The $\text{Log } D_{7.4}$ values of [^{68}Ga]Ga-PP4-WD and [^{68}Ga]Ga-PP8-WD were -3.06 ± 0.15 and -4.27 ± 0.26 , respectively (Table 1). These results indicate

that $[^{68}\text{Ga}]\text{Ga-PP8-WD}$ is more hydrophilic than $[^{68}\text{Ga}]\text{Ga-PP4-WD}$.

Stability

The stability of both $[^{68}\text{Ga}]\text{Ga-PP4-WD}$ and $[^{68}\text{Ga}]\text{Ga-PP8-WD}$ was investigated by incubating each radioligand in either PBS or human serum at 37 °C (Fig. 4). After 2 h of incubation, the radiochemical purity of two radiotracers was slightly reduced in the PBS medium but still remained as high as 97%. Both radiotracers demonstrated remarkable stability in human serum, as indicated by the radiochemical purity of $[^{68}\text{Ga}]\text{Ga-PP4-WD}$

and $[^{68}\text{Ga}]\text{Ga-PP8-WD}$ remaining at $96.83 \pm 0.87\%$ and $96.69 \pm 0.21\%$ at 2 h, respectively.

Cell affinity studies

The specific cell surface binding and internalization into LNCaP cells were determined for $[^{68}\text{Ga}]\text{Ga-PP4-WD}$ and $[^{68}\text{Ga}]\text{Ga-PP8-WD}$ with $[^{68}\text{Ga}]\text{Ga-Flu-1}$ as a reference. As shown in Fig. 5, both uptake and internalization of three radioligands displayed a time-dependent pattern and rose over 120 min duration. Specifically, the uptake and internalization of $[^{68}\text{Ga}]\text{Ga-PP4-WD}$ reached $26.30 \pm 2.06\%$ and $9.36 \pm 1.70\%$ after 120 min

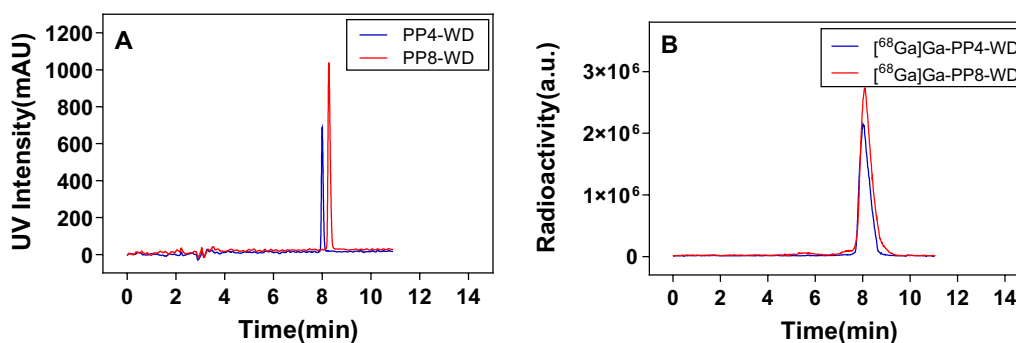


Fig. 3 HPLC chromatogram of PP4-WD, PP8-WD (A) and Radio-HPLC chromatogram of $[^{68}\text{Ga}]\text{Ga-PP4-WD}$, $[^{68}\text{Ga}]\text{Ga-PP8-WD}$ (B)

Table 1 Analytical data of PP4-WD, PP8-WD, and Flu-1

Compound	Chemical formula	Calculated mass	m/z ¹	tr (min) ²	Radiochemical purity (%) ³	Log D _{7,4}
PP4-WD	C ₅₄ H ₇₉ N ₉ O ₂₀	1174.27	1174.55	8.01	97.98 ± 0.56	-3.06 ± 0.15
PP8-WD	C ₆₂ H ₉₅ N ₉ O ₂₄	1350.48	1350.66	8.09	96.56 ± 0.32	-4.23 ± 0.26
Flu-1 ⁴	C ₄₇ H ₆₆ N ₈ O ₁₅	983.43	983.47	8.13	88.53 ± 1.21	-2.64 ± 0.25

¹ Mass spectrometry data detected as $[\text{M} + \text{H}]^+$. ²Retention times of the Ga-labeled compounds. ³Values of radiochemical purity were measured by RP-HPLC. An Agilent analytical column (250 × 4.6 mm) was utilized with mobile phases consisting of 0.1% TFA in water (A) and ACN (B). A linear gradient of solvent A (90–10% in 15 min) in solvent B (10–90% in 15 min) at a flow rate of 1.0 mL/min. ⁴Data for $[^{68}\text{Ga}]\text{Ga-Flu-1}$ was obtained from a previously published report [21]

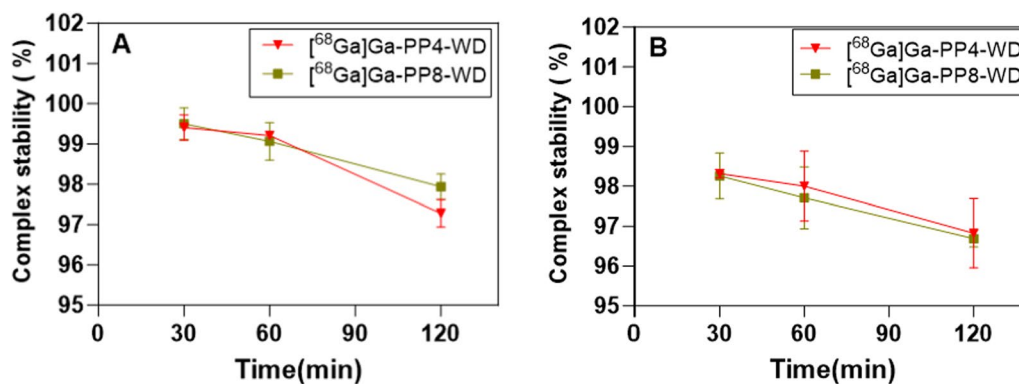


Fig. 4 Stability of $[^{68}\text{Ga}]\text{Ga-PP4-WD}$ and $[^{68}\text{Ga}]\text{Ga-PP8-WD}$. Radiochemical purity was recorded in PBS (A) and human serum (B) at 30, 60, and 120 min

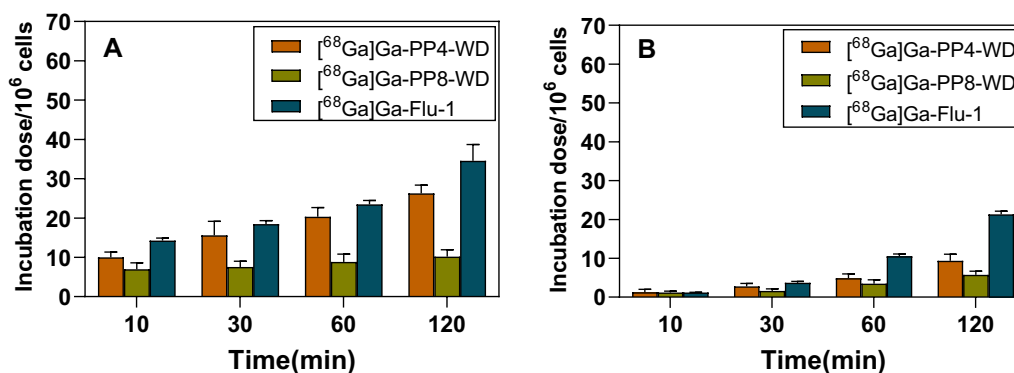


Fig. 5 The uptake (A) and internalization (B) of $[^{68}\text{Ga}]\text{Ga-PP4-WD}$, $[^{68}\text{Ga}]\text{Ga-PP8-WD}$, and $[^{68}\text{Ga}]\text{Ga-Flu-1}$ in LNCaP cells (~240,000 cells/well, normalized to 10^6 cells) at 10, 30, 60, and 120 min

of incubation, respectively. Under the same condition, $[^{68}\text{Ga}]\text{Ga-PP8-WD}$ exhibited only moderate uptake and internalization rates, measuring at $10.16 \pm 1.87\%$ and $5.72 \pm 0.95\%$, respectively, with a gradual increase observed over the same period. In contrast, $[^{68}\text{Ga}]\text{Ga-Flu-1}$ demonstrated rapid enhancement in both uptake and internalization levels throughout the course of the experiments and eventually reached $34.57 \pm 4.14\%$ and $21.3 \pm 0.13\%$, respectively, at 120 min. Overall, all three radioligands displayed increasing uptake and internalization levels over the course of experiments. Compared to the other two radioligands under the same conditions, $[^{68}\text{Ga}]\text{Ga-Flu-1}$ revealed higher uptake and internalization levels.

The binding affinity of $[^{68}\text{Ga}]\text{Ga-PP4-WD}$ and $[^{68}\text{Ga}]\text{Ga-PP8-WD}$ was measured by in vitro competition binding assays using PSMA-expressing LNCaP cells and $[^{68}\text{Ga}]\text{Ga-PSMA-11}$ as the reference compound. As shown in Additional file 1: Figure S3, both compounds competitively inhibited binding with $[^{68}\text{Ga}]\text{Ga-PSMA-11}$ to LNCaP cells in a dose-dependent manner. The calculated IC_{50} values for $[^{68}\text{Ga}]\text{Ga-PP4-WD}$, $[^{68}\text{Ga}]\text{Ga-PP8-WD}$, and $[^{68}\text{Ga}]\text{Ga-Flu-1}$ were 8.06 ± 0.91 , 6.13 ± 0.79 , and 9.62 ± 1.70 nM [20], respectively.

Biodistribution

Biodistribution was conducted to evaluate the major organ distribution profile of radiotracers in LNCaP tumor-bearing NOD/SCID mice. $[^{68}\text{Ga}]\text{Ga-Flu-1}$ was examined as the positive control, which was reported by our group previously [21]. The results were decay-corrected, listed as a percentage of the injected activity per gram of tissue mass (%ID/g), and presented as the average \pm standard deviation (SD) (Fig. 6, Additional file 1: Tables S1–S3).

The results indicated that all radioligands exhibited high specific uptake and rapid accumulation in LNCaP

tumors. After 30 min, the radioactivity accumulation of the three radioligands, namely $[^{68}\text{Ga}]\text{Ga-PP4-WD}$, $[^{68}\text{Ga}]\text{Ga-PP8-WD}$, and $[^{68}\text{Ga}]\text{Ga-Flu-1}$, was found to be $33.45 \pm 3.40\% \text{ID/g}$, $16.18 \pm 2.53\% \text{ID/g}$, and $32.86 \pm 12.02\% \text{ID/g}$, respectively. Furthermore, tumor uptake continued to increase over time, as demonstrated by the values of $39.28 \pm 3.25\% \text{ID/g}$, $18.64 \pm 2.20\% \text{ID/g}$, and $52.07 \pm 14.83\% \text{ID/g}$ at 60 min. However, these values decreased to $25.75 \pm 2.43\% \text{ID/g}$, $17.12 \pm 2.57\% \text{ID/g}$, and $40.11 \pm 9.24\% \text{ID/g}$ at 120 min.

The results showed that renal pathway is the primary route of excretion for all three radioligands. Specifically, the renal uptake of $[^{68}\text{Ga}]\text{Ga-PP4-WD}$ and $[^{68}\text{Ga}]\text{Ga-PP8-WD}$ was significantly reduced compared to $[^{68}\text{Ga}]\text{Ga-Flu-1}$. The uptake values at 30 min were $47.24 \pm 3.68\% \text{ID/g}$ for $[^{68}\text{Ga}]\text{Ga-PP8-WD}$ and $25.63 \pm 3.46\% \text{ID/g}$ for $[^{68}\text{Ga}]\text{Ga-PP4-WD}$, and $240.00 \pm 34.68\% \text{ID/g}$ for $[^{68}\text{Ga}]\text{Ga-Flu-1}$. While the accumulated activity in kidneys decreased over time for all three radioligands, it remained relatively high for $[^{68}\text{Ga}]\text{Ga-Flu-1}$ at $127.83 \pm 27.94\% \text{ID/g}$, in contrast, there was a substantial reduction in accumulated activity for both $[^{68}\text{Ga}]\text{Ga-PP4-WD}$ and $[^{68}\text{Ga}]\text{Ga-PP8-WD}$, with values of $2.23 \pm 0.58\% \text{ID/g}$ and $6.39 \pm 1.56\% \text{ID/g}$, respectively. For other normal organ/tissues, the radioactivity accumulated was rapidly eliminated.

In contrast to the biodistribution results of the LNCaP model, $[^{68}\text{Ga}]\text{Ga-PP4-WD}$ and $[^{68}\text{Ga}]\text{Ga-PP8-WD}$ tumors were slightly decreased in the PC3-PIP tumor model. The uptake of $[^{68}\text{Ga}]\text{Ga-PP4-WD}$ and $[^{68}\text{Ga}]\text{Ga-PP8-WD}$ in tumors was $27.43 \pm 1.81\% \text{ID/g}$ and $15.21 \pm 3.33\% \text{ID/g}$, respectively, compared to the uptake values of $39.28 \pm 3.25\% \text{ID/g}$ and $18.64 \pm 2.20\% \text{ID/g}$ in LNCaP tumor mice model, respectively. However, the trend of tumor uptake at each time point was the same as in the LNCaP model, such that although renal uptake of $[^{68}\text{Ga}]\text{Ga-PP4-WD}$ was higher than $[^{68}\text{Ga}]\text{Ga-PP8-WD}$

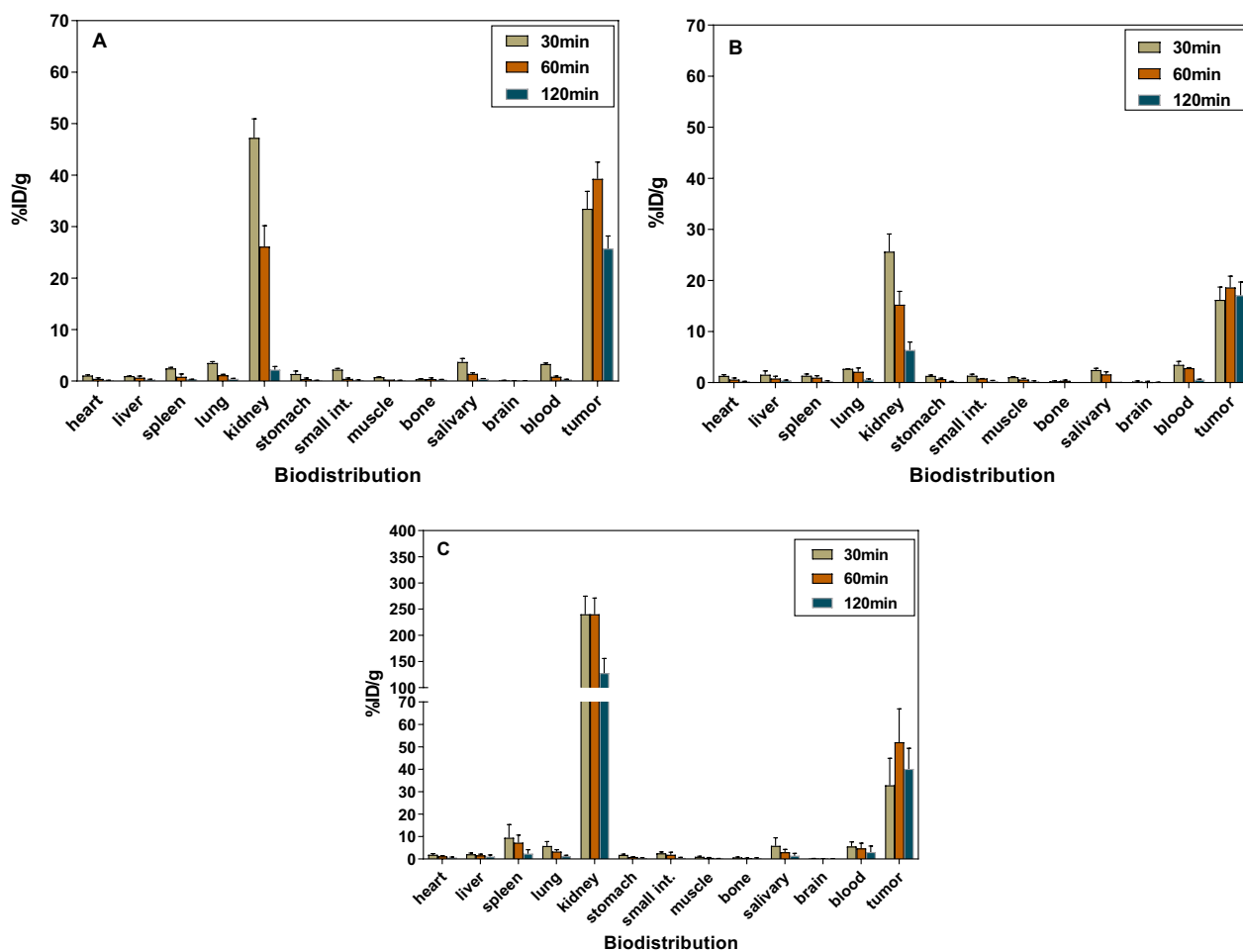


Fig. 6 Organ biodistribution of [^{68}Ga]Ga-PP4-WD (A), [^{68}Ga]Ga-PP8-WD (B), and [^{68}Ga]Ga-Flu-1 (C) in LNCaP tumor model expressed as %ID/g tissue at 30, 60, and 120 min post-injection (p.i.) Data are expressed as the mean \pm SD ($n=5$). small int. = small intestine

at 30 min, renal uptake of [^{68}Ga]Ga-PP4-WD was lower than [^{68}Ga]Ga-PP8-WD after 60 min and 120 min. In the PC3-PIP model, the peak uptake was still around 60 min, while the tumor uptake of [^{68}Ga]Ga-PP4-WD was also higher than the [^{68}Ga]Ga-PP8-WD at the corresponding time points, which is consistent with the characteristics in the LNCaP model. In addition, according to the biodistribution results of the PC3-PIP model, the overall uptake of [^{68}Ga]Ga-PP8-WD was increased slightly in non-target organs, but these increases were all small or even negligible (Additional file 1: Figure S4, Tables S7–S8).

Tumor-to-normal tissue (T/N)

The biodistribution data in LNCaP tumor model at 30, 60, and 120 min were used to calculate the ratios of tumors to key normal organs (Fig. 7, Additional file 1: Tables S4–S6). As illustrated in Fig. 7, within a two-hour time course, the ratios for target organs exhibited

a consistent upward trend for all three radioligands. Interestingly, the data indicated that while the tumor uptake of [^{68}Ga]Ga-PP4-WD is lower than that of [^{68}Ga]Ga-Flu-1, the T/N ratios for [^{68}Ga]Ga-PP4-WD in all selected organs are significantly higher than that of both [^{68}Ga]Ga-PP8-WD and [^{68}Ga]Ga-Flu-1.

Micro-PET/CT imaging

NOD/SCID mice bearing LNCaP tumors were selected for the whole-body micro-PET/CT imaging study of [^{68}Ga]Ga-PP4-WD, [^{68}Ga]Ga-PP8-WD, and the reference radiotracer [^{68}Ga]Ga-Flu-1.

To evaluate the specificity of radioligands, blocking experiments were performed. In brief, 40 nmol of the PSMA inhibitor 2-PMPA was administered, followed by the injection of approximately 2.6 MBq of radioligands after 30 min. Then a static scan of micro-PET/CT was performed 60 min later. Upon blocking, it was observed that there was substantially reduced radioactivity

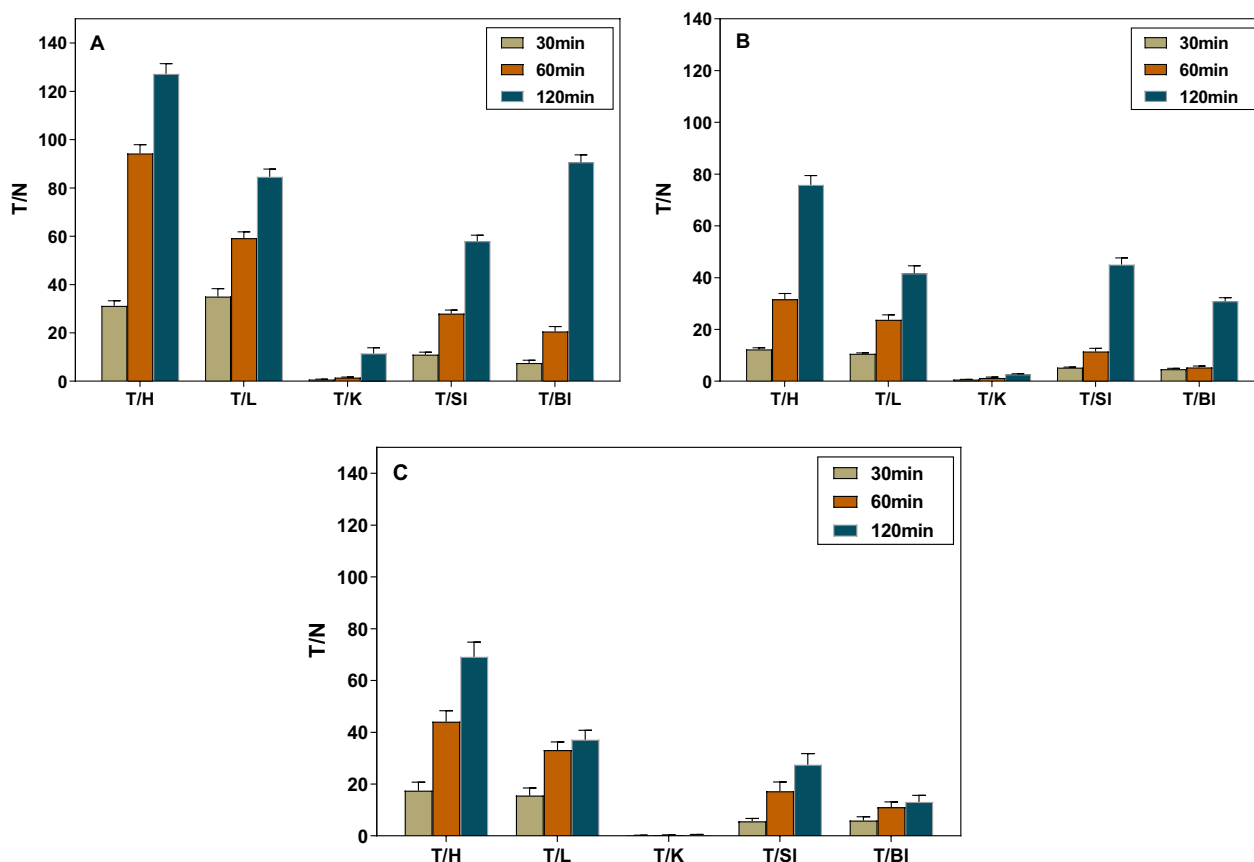


Fig. 7 The tumor-to-heart (T/H), tumor-to-liver (T/L), tumor-to-kidney (T/K), tumor-to-salivary (T/SI) and tumor-to-blood (T/BI) values at 30, 60, and 120 min were obtained from the biodistribution data of [⁶⁸Ga]Ga-PP4-WD (A), [⁶⁸Ga]Ga-PP8-WD (B), and [⁶⁸Ga]Ga-Flu-1 (C) in LNCaP tumor model

detected for both [⁶⁸Ga]Ga-PP4-WD and [⁶⁸Ga]Ga-PP8-WD (Additional file 1: Figure S5A, S5B). Meanwhile, no significant reduction in uptake within normal organs, indicating the exceptional specificity of [⁶⁸Ga]Ga-PP4-WD and [⁶⁸Ga]Ga-PP8-WD for LNCaP tumors. In parallel, we conducted blocking imaging of PC3-PIP using the identical methodology as previously described, and the outcomes were in concordance with those observed in the LNCaP tumor model (Additional file 1: Figure S5C, S5D). This consistency underscores the remarkable specificity of [⁶⁸Ga]Ga-PP4-WD and [⁶⁸Ga]Ga-PP8-WD for PSMA-positive tumors.

Time-dependent static scans were performed for [⁶⁸Ga]Ga-PP4-WD, [⁶⁸Ga]Ga-PP8-WD, and [⁶⁸Ga]Ga-Flu-1 at 10, 30, 60, and 120 min (Fig. 8, Additional file 1: Figure S6). These radioligands exhibited rapid accumulation in PSMA-positive LNCaP tumors as early as 10 min p.i., and by 120 min, all radioligands showed a clean background. Consistent with the biodistribution data, radioactivity for [⁶⁸Ga]Ga-PP4-WD and [⁶⁸Ga]Ga-PP8-WD was swiftly cleared from renal. In contrast, [⁶⁸Ga]

Ga-Flu-1 demonstrated a significantly higher level of accumulated radioactivity in the renal area throughout the experiment.

Following the static PET scan, a dynamic PET scan was performed to understand the pharmacokinetics of these radiotracers (Fig. 9). The dynamic uptake curves over a 2-h period revealed their fast-targeting properties, as the radiotracers quickly accumulated in the tumor and remained increasing uptake throughout the experiment. In terms of renal uptake, both [⁶⁸Ga]Ga-PP4-WD and [⁶⁸Ga]Ga-PP8-WD revealed an initial increase followed by a subsequent decrease. In contrast, the accumulation of [⁶⁸Ga]Ga-Flu-1 exhibited a continually ascending pattern. Furthermore, both [⁶⁸Ga]Ga-PP4-WD and [⁶⁸Ga]Ga-PP8-WD displayed superior renal clearance compared with [⁶⁸Ga]Ga-Flu-1. Dynamic coronal fused micro-PET/CT images obtained after injection of [⁶⁸Ga]Ga-PP4-WD (A), [⁶⁸Ga]Ga-PP8-WD (B), and [⁶⁸Ga]Ga-Flu-1 (C) in LNCaP tumor model over 2 h were performed in supplementary information (Additional file 1: Figure S7).

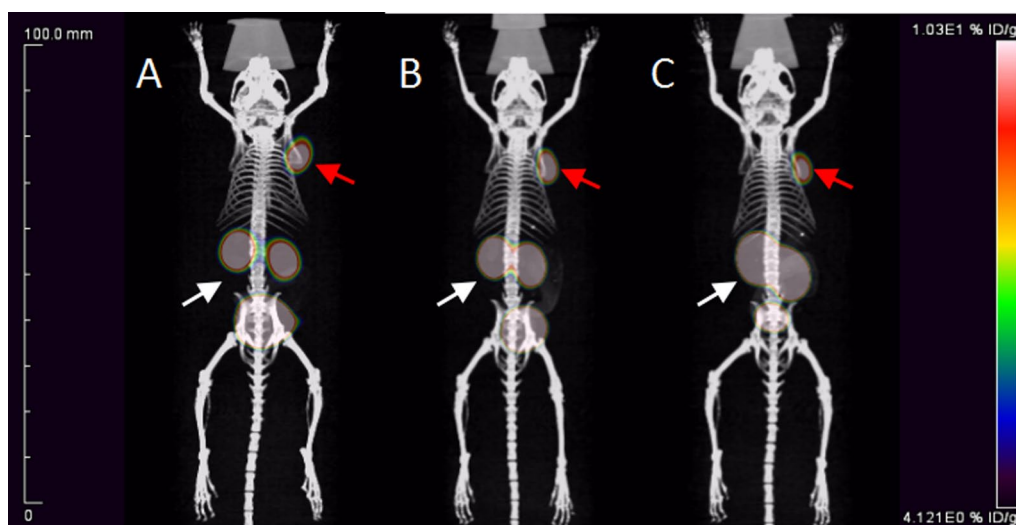


Fig. 8 Maximum intensity projections of whole-body coronal micro-PET/CT images of a NOD/SCID male mouse bearing an LNCaP tumor xenograft (red arrow for the tumor, white arrow for the kidney). The tumor-targeting efficacy of $[^{68}\text{Ga}]\text{Ga-PP4-WD}$, $[^{68}\text{Ga}]\text{Ga-PP8-WD}$ and $[^{68}\text{Ga}]\text{Ga-Flu-1}$ was demonstrated by time-dependent static scans at 60 min p.i. of $[^{68}\text{Ga}]\text{Ga-PP4-WD}$ (A), $[^{68}\text{Ga}]\text{Ga-PP8-WD}$ (B), and $[^{68}\text{Ga}]\text{Ga-Flu-1}$ (C). Approximately 2.6 MBq was injected into each mouse

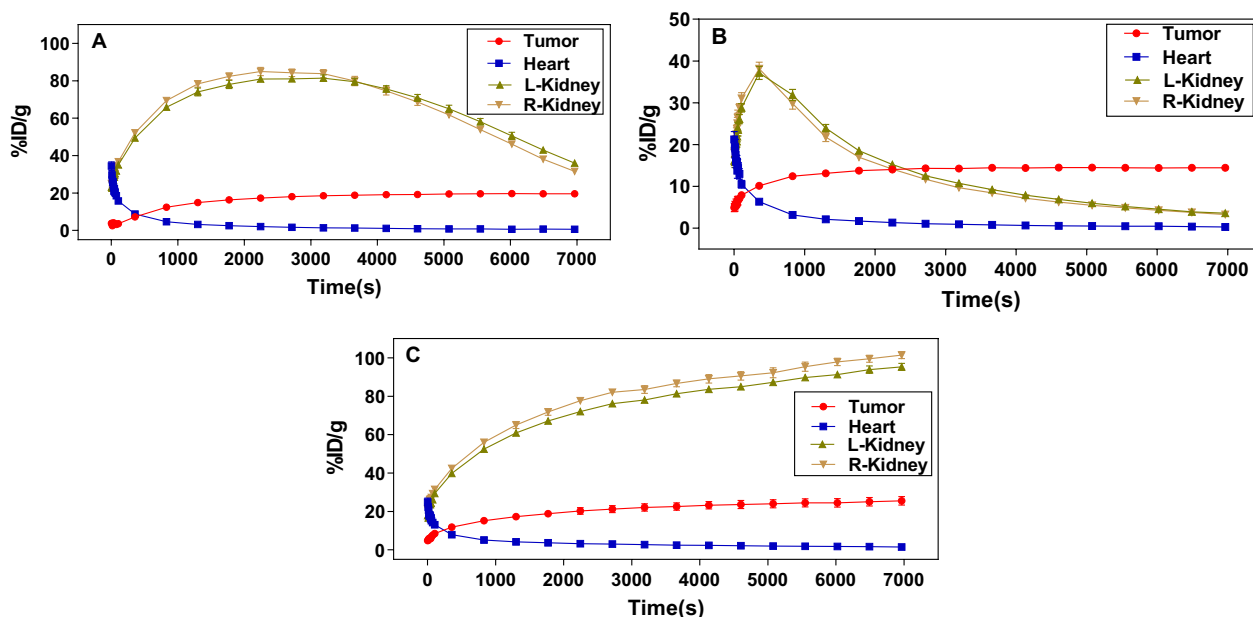


Fig. 9 %ID/g (mean) was obtained from the whole-body coronal micro-PET/CT scans of the NOD/SCID male mice bearing LNCaP tumor xenografts. The tumor-targeting efficacies of $[^{68}\text{Ga}]\text{Ga-PP4-WD}$ (A), $[^{68}\text{Ga}]\text{Ga-PP8-WD}$ (B), and $[^{68}\text{Ga}]\text{Ga-Flu-1}$ (C) were demonstrated by dynamic micro-PET scans

Micro-SPECT/CT imaging

Balb/c-nu mice carrying PC3-PIP tumors were chosen for the micro-SPECT/CT imaging investigation of $[^{177}\text{Lu}]\text{Lu-PP4-WD}$ and $[^{177}\text{Lu}]\text{Lu-PP8-WD}$ (see Additional file 1: Figure S8). The findings indicated that,

under the same parameters. Both radioligands exhibited rapid targeted uptake and maintained a favorable tumor-to-background ratio for up to 168 h, with minimal observable uptake in non-target organs, except for the bladder.

Discussion

In previous work, we developed a PSMA-targeted inhibitor called [^{68}Ga]Ga-Flu-1, which utilized a Lys-urea-Glu backbone and demonstrated excellent specificity and affinity in vivo for PSMA. However, we also observed a significant disparity in uptake between the kidneys and prostate tumor, with the kidneys showing much higher levels of [^{68}Ga]Ga-Flu-1. The elevated uptake in kidneys raises concern about its potential impact on renal function and its potential to hinder the precise detection of kidney metastases in the cases where such metastases are present. PEG chains were often used as linkers to improve the hydrophilicity and the circulation time of the radiotracer in blood, leading to diverse biodistribution of the radiotracer [28, 29]. The lengths of PEG chains might have significantly impact on various biological properties of the drug, including hydrophilicity [30], absorption or release [31], blood circulation, and targeting ability with a size-dependent pattern [32, 33]. Lee W et al. showed that a PEGylated antibody cleared much faster from the blood while maintaining tumor uptake compared to its non-PEGylated counterpart [34]. In this study, the compounds with PEG chains containing four repeat units of middle size and eight repeat units of larger size were incorporated, and compared with non-PEGylated ligand, the in vitro and in vivo properties were examined.

The results revealed that introducing PEG chain had a noticeable impact on the physicochemical properties of the compound, leading to significant impact on its in vitro and in vivo properties. Specifically, the water solubility, as expected, was enhanced after PEG modification, as indicated by the decrease in $\text{LogD}_{7.4}$ value from -2.64 ± 0.25 for the unmodified [^{68}Ga]Ga-Flu-1 to -4.23 ± 0.26 for [^{68}Ga]Ga-PP8-WD, demonstrating a considerable improvement in water solubility. Accordingly, biodistribution properties of both radiotracers have undergone significant alterations, such as renal uptake, in particular, reduced by a factor of 40 and 20 at 120 min p.i. compared to [^{68}Ga]Ga-Flu-1, respectively. Radioactivity accumulation in other normal organs like liver, was slightly reduced as well. Statistical analysis revealed that the uptake of [^{68}Ga]Ga-Flu-1 in LNCaP tumor was significantly higher than [^{68}Ga]Ga-PP8-WD at 60 min p.i. ($P < 0.05$). However, there was no significant difference between [^{68}Ga]Ga-PP4-WD and [^{68}Ga]Ga-Flu-1 ($P > 0.05$). The renal uptake of both [^{68}Ga]Ga-PP4-WD and [^{68}Ga]Ga-PP8-WD was significantly lower than for [^{68}Ga]Ga-Flu-1 ($P < 0.05$) at given time points. These results indicated that PEG-modified compounds can effectively facilitate the renal clearance and reduce their uptake in the kidneys, likely by reduced tubular reabsorption, decreased binding to renal transporters, or rapid kidney filtration of the radioligands.

Whole body coronal micro-PET/CT static images of NOD/SCID male mice carrying LNCaP tumor xenografts had a clean background and high image quality. Combined with the dynamic uptake profile, it is evident that [^{68}Ga]Ga-PP4-WD and [^{68}Ga]Ga-PP8-WD were metabolized via kidneys as evidenced by a rapid decline of radioactivity within 2 h. In addition, when considering the dynamic uptake curves and the ability to effectively block tumor visualization in mice with tumors, both [^{68}Ga]Ga-PP4-WD and [^{68}Ga]Ga-PP8-WD highlighted the excellent specificity and quick targeting property for PSMA. These findings align with biodistribution results. Therefore, the substitution of the linker group with PEG remained the targeting characteristics while significantly decreasing renal uptake of the radiotracers. Although there was a slight decrease in tumor uptake, this was offset by reduced uptake in normal organs. As a result, these radiotracers still achieved impressive T/N (tumor-to-normal) values and image contrast.

Conclusion

In summary, we have successfully developed two [^{68}Ga]Ga-labeled PSMA-targeted radiotracers featuring PEG-modified chains. These radiotracers have demonstrated their effectiveness in significantly reducing kidney uptake while maintaining the absorbed dose in tumors. Both radiotracers exhibited strong binding and internalization characteristics in vitro, displayed high specificity and affinity for PSMA in vivo. Notably, [^{68}Ga]Ga-PP4-WD, in particular, holds promise as a potential new diagnostic PET tracer for prostate cancer.

Supplementary Information

The online version contains supplementary material available at <https://doi.org/10.1186/s13550-024-01071-z>.

Additional file 1. The synthesis, characterization, IC50 measurements, biodistribution data, and small animal PET/CT images of these radiotracers.

Acknowledgements

The authors would like to thank the National Natural Science Foundation of China for funding this work (U20A20384); the Doctoral Research Initiation Fund of Affiliated Hospital of Southwest Medical University; Natural Science Foundation of Sichuan Province grant (2023NSFSC0635); the Sichuan Science and Technology Foundation (2021YJ0131 and 2020ZYD101); Luzhou-Southwest Medical University Cooperative Application Foundation (2020LZXNYDJ50), Science and Technology Project of Sichuan Province (2022YFS0608), and Science and Technology Project of Luzhou (2021LZXNYD-C02).

Author contributions

The study was designed by ZJZ and YC. Material preparation, data collection, and analysis were performed by YL, LX, YF, HYL, PC, GFL, SFT, and NL. The manuscript was written and reviewed by YL and ZJZ. Funding acquisition was by YC, ZJZ, GFL, and WZ. All authors read and approved the final manuscript. All methods were carried out following relevant guidelines and regulations, and all methods are reported per ARRIVE guidelines.

Funding

The National Natural Science Foundation of China for funding this work (U20A20384); the Doctoral Research Initiation Fund of Affiliated Hospital of Southwest Medical University; Natural Science Foundation of Sichuan Province grant (2023NSFSC0635); the Sichuan Science and Technology Foundation (2021YJ0131 and 2020ZYD101); Luzhou-Southwest Medical University Cooperative Application Foundation (2020LZXNYDJ50), Science and Technology Project of Sichuan Province (2022YF50608), and Science and Technology Project of Luzhou (2021LZXNYD-C02).

Declarations

Ethics approval and consent to participate

The Ethics Committee for Southwest Medical University (2022-03-22) approved the study. All methods were carried out in accordance with relevant guidelines and regulations. The study was carried out compliance with the ARRIVE guidelines.

Consent for publication

Not Applicable.

Availability of data and materials

The datasets used and/or analyzed during the current study available from the corresponding author on reasonable request.

Competing interests

The authors declare no conflict of interest.

Author details

¹Department of Nuclear Medicine, The Affiliated Hospital, Southwest Medical University, Jiangyang District, Luzhou, Sichuan, China. ²Nuclear Medicine and Molecular Imaging Key Laboratory of Sichuan Province, Department of Nuclear Medicine, The Affiliated Hospital, Southwest Medical University, Jiangyang District, Luzhou, Sichuan, China. ³Institute of Nuclear Medicine, Southwest Medical University, Jiangyang District, Luzhou, Sichuan, China. ⁴Department of Pharmaceutics, School of Pharmacy, Southwest Medical University, Jiangyang District, Luzhou, Sichuan, China. ⁵Department of Nuclear Medicine, Sichuan Provincial People's Hospital, University of Electronic Science and Technology of China, Sichuan, Chengdu, China.

Received: 25 October 2023 Accepted: 24 January 2024

Published online: 07 February 2024

References

- Siegel RL, Miller KD, Fuchs HE, Jemal A. Cancer statistics, 2022. *CA Cancer J Clin.* 2022;72(1):7–33.
- Siegel RL, Miller KD, Wagle NS, Jemal A. Cancer statistics, 2023. *CA Cancer J Clin.* 2023;73(1):17–48. <https://doi.org/10.3322/caac.21763>. (PMID: 36633525).
- Auchus RJ, Sharif N. Sex hormones and prostate cancer. *Annu Rev Med.* 2020;71:33–45.
- Chatalic KL, Konijnenberg M, Nonnekens J, et al. *In vivo* stabilization of a gastrin-releasing peptide receptor antagonist enhances PET imaging and radionuclide therapy of prostate cancer in preclinical studies. *Theranostics.* 2016;6(1):104–17.
- Kim MM, Hoffman KE, Levy LB, et al. Improvement in prostate cancer survival over time. *Cancer J.* 2012;18:1–8.
- Edwards BK, Noone AM, Mariotto AB, et al. Annual Report to the Nation on the status of cancer, 1975–2010, featuring prevalence of comorbidity and impact on survival among persons with lung, colorectal, breast, or prostate cancer. *Cancer.* 2014;120:1290–314.
- Thompson IM, Tangen CM. Prostate cancer screening comes of age. *Lancet.* 2014;384:2004–6.
- Tsechlidis I, Vrachimis A. PSMA PET in imaging prostate cancer. *Front Oncol.* 2022;12: 831429.
- Chang SS. Overview of prostate-specific membrane antigen. *Rev Urol.* 2004;6(Suppl 10):S13–8.
- Silver DA, Pellicer I, Fair WR, Heston WD, Cordon-Cardo C. Prostate-specific membrane antigen expression in normal and malignant human tissues. *Clin Cancer Res.* 1997;3(1):81–5.
- Bostwick DG, Pacelli A, Blute M, Roche P, Murphy GP. Prostate specific membrane antigen expression in prostatic intraepithelial neoplasia and adenocarcinoma: a study of 184 cases. *Cancer.* 1998;82(11):2256–61.
- Eder M, Eisenhut M, Babich J, Haberkorn U. PSMA as a target for radiolabeled small molecules. *Eur J Nucl Med Mol Imaging.* 2013;40(6):819–23.
- Ghosh A, Heston WD. Tumor target prostate specific membrane antigen (PSMA) and its regulation in prostate cancer. *J Cell Biochem.* 2004;91:528–39.
- Kinoshita Y, Kuratsukuri K, Landas S, et al. Expression of prostate-specific membrane antigen in normal and malignant human tissues. *World J Surg.* 2006;30:628–36.
- Barve A, Jin W, Cheng K. Prostate cancer relevant antigens and enzymes for targeted drug delivery. *J Control Release.* 2014;187:118–32.
- Kiess AP, Banerjee SR, Mease RC, et al. Prostate-specific membrane antigen as a target for cancer imaging and therapy. *Q J Nucl Med Mol Imaging.* 2015;59(3):241–68.
- Perera M, Papa N, Roberts M, et al. Gallium-68 prostate-specific membrane antigen positron emission tomography in advanced prostate cancer—updated diagnostic utility, sensitivity, specificity, and distribution of prostate-specific membrane antigen-avid lesions: a systematic review and meta-analysis. *Eur Urol.* 2020;77(4):403–41710.
- Maurer T, Eiber M, Schwaiger M, Gschwend JE. Current use of PSMA-PET in prostate cancer management. *Nat Rev Urol.* 2016;13(4):226–35.
- Jeitner TM, Babich JW, Kelly JM. Advances in PSMA theranostics. *Transl Oncol.* 2022;22: 101450.
- Fallah J, Agrawal S, Gittleman H, et al. FDA approval summary: lutetium Lu 177 vipivotide tetraxetan for patients with metastatic castration-resistant prostate cancer. *Clin Cancer Res.* 2023;29(9):1651–7. <https://doi.org/10.1158/1078-0432.CCR-22-2875>.
- Cai P, Tang S, Xia L, Wang Y, Liu Y, Feng Y, Liu N, Chen Y, Zhou Z. Improve the biodistribution with bulky and lipophilic modification strategies on Lys-Urea-Glu-based PSMA-targeting radiotracers. *Mol Pharm.* 2023;11:1. <https://doi.org/10.1021/acs.molpharmaceut.2c01101>. (PMID: 36696174).
- Kurtul N, Resim S, Koçarslan S. Giant renal metastasis from prostate cancer mimicking renal cell carcinoma. *Turk J Urol.* 2018;44(4):367–9. <https://doi.org/10.5152/tud.2017.39225>.
- Canalle LA, Löwik DWPM, van Hest JCM. Polypeptide–polymer bioconjugates. *Chem Soc Rev.* 2010;39:329–53.
- Wirth P, Soupe J, Tritsch D, Biellmann JF. Chemical modification of horseradish peroxidase with ethanal-methoxypolyethylene glycol: solubility in organic solvents, activity, and properties. *Bioorg Chem.* 1991;19:133–42.
- Kinstler OB, Brems DN, Lauren SL, Paige AG, Hamburger JB, Treuheit MJ. Exploring the impact of PEGylation on pharmacokinetics: a size-dependent effect of polyethylene glycol on prostate specific membrane antigen inhibitors. *Pharm Res.* 1996;13:996–1002.
- Caliceti P, Veronese FM. Pharmacokinetic and biodistribution properties of poly (ethylene glycol)–protein conjugates. *Adv Drug Delivery Rev.* 2003;55:1261–77.
- Liu Y, Xia L, Cai P, et al. In vitro and in vivo comparative study of 68Ga-labeled DOTA-, NOTA-, and HBEDCC-chelated radiotracers targeting prostate-specific membrane antigen. *J Radioanal Nucl Chem.* 2023;332:617–28. <https://doi.org/10.1007/s10967-022-08731-1>.
- Ginn C, et al. PEGylation and its impact on the design of new protein-based medicines. *Fut Med Chem.* 2014;6(16):1829–46.
- Cao D, et al. Divalent folate modification on PEG: an effective strategy for improving the cellular uptake and targetability of PEGylated polyamidoamine–polyethylenimine copolymer. *Mol Pharm.* 2015;12(1):240–52.
- Chan P, et al. Synthesis and characterization of chitosan-g-poly (ethylene glycol)-folate as a non-viral carrier for tumor-targeted gene delivery. *Biomaterials.* 2007;28(3):540–9.
- Papadimitriou SA, et al. Chitosan-g-PEG nanoparticles ionically crosslinked with poly (glutamic acid) and triphosphosphate as protein delivery systems. *Int J Pharm.* 2012;430(1–2):318–27.
- Yang C, et al. Impact of PEG chain length on the physical properties and bioactivity of PEGylated chitosan/siRNA nanoparticles in vitro and in vivo. *ACS Appl Mater Interfaces.* 2017;9(14):2203–16.

33. Chen J, et al. Methotrexate-loaded PEGylated chitosan nanoparticles: synthesis, characterization, and in vitro and *in vivo* antitumoral activity. *Mol Pharm*. 2014;11(7):2213–23.
34. Lee W, Bobba KN, Kim JY, et al. A short PEG linker alters the in vivo pharmacokinetics of trastuzumab to yield high-contrast immuno-PET images [published correction appears in *J Mater Chem B*. 2021 Aug 4;9(30):6092]. *J Mater Chem B*. 2021;9(13):2993–7. <https://doi.org/10.1039/d0tb02911d>.

Publisher's Note

Springer Nature remains neutral with regard to jurisdictional claims in published maps and institutional affiliations.